ELSEVIER

Tectonophysics 348 (2002) 205–218

TECTONOPHYSICS

www.elsevier.com/locate/tecto

Magma-induced strain localization in centrifuge models of transfer zones

Giacomo Corti [a,*], Marco Bonini [b], Francesco Mazzarini [c], Mario Boccaletti [d], Fabrizio Innocenti [a], Piero Manetti [d,e], Genene Mulugeta [f], Dimitrios Sokoutis [g]

[a] *Dipartimento di Scienze della Terra, Università degli Studi di Pisa, via S. Maria, 53, 56126 Pisa, Italy*
[b] *Instituto di Geoscienze e Georisorse (I.G.G.-CNR), Sezione di Firenze, via La Pira, 4, 50121 Firenze, Italy*
[c] *Instituto di Geoscienze e Georisorse (I.G.G.-CNR) Sede, c/o Dipartimento di Scienze della Terra, Università degli Studi di Pisa, via di S. Maria, 53, 56126 Pisa, Italy*
[d] *Instituto di Geoscienze e Georisorse (I.G.G.-CNR) Sede, via G. Moruzzi, 1, 56124 Pisa, Italy*
[e] *Dipartimento di Scienze della Terra, Università degli Studi di Firenze, via La Pira, 4, 50121 Florence, Italy*
[f] *Hans Ramberg Tectonic Laboratory, Institute of Earth Sciences, Uppsala University, Villavagen 16, 752 36 Uppsala, Sweden*
[g] *Netherlands Center for Integrated Earth Sciences, Faculty of Earth Sciences, Vrije Universiteit Amsterdam, De Boelelaan 1085, 1081 HV, Amsterdam, The Netherlands*

Accepted 18 January 2002

Abstract

Scaled centrifuge experiments have been used to investigate the dynamic relations between deformation and magma distribution in rift-related transfer zones. The physical models were built using suitable analogue materials, such as sand to represent the brittle upper crust, various kinds of silicone mixtures to simulate the lower crust and upper mantle and glycerol to reproduce magma. Models simulated the development of transfer zones across pre-existing glycerol reservoirs placed at the base of the analogue continental crust. In plan view, different geometries, dimensions and positions of subcrustal reservoirs were reproduced in three different sets of experiments; to compare results, models were also performed without magma-simulating glycerol. Set 1 experiments, incorporating a narrow rectangular glycerol reservoir, show that the low-viscosity material is able to localise deformation into the overlying crust, giving rise to discrete transfer zones. This concentrated surface deformation corresponds at depth to major magma accumulation. Set 2 experiments, with an initial wide squared glycerol reservoir, show instead that deformation is distributed across the whole model surface, corresponding at depth to relatively minor magma accumulation. Set 3 experiments explored various positions of a small squared reservoir that invariably localised faulting in the overlying analogue brittle crust at the onset of model deformation. The overall model behaviour suggests that magma distribution at depth can effectively control the strain distribution in the overlying crust and the deformative pattern of transfer zones. Strain distribution, in turn, may control magma emplacement as localized deformation would favour major accumulation of magma at transfer zones. Coupled to a strong thermal weakening of the country rocks, this process may ultimately lead to a positive feedback interaction between magma and deformation.

Keywords: Transfer zones; Strain localisation; Magma emplacement; Centrifuge models

* Corresponding author. Tel.: +39-50-847-260.
E-mail address: corti@dst.unipi.it (G. Corti).

0040-1951/02/$ - see front matter
PII: S0040-1951(02)00063-X

1. Introduction

Continental rifts are often segmented by transfer zones in which boundary faults interact to conserve extensional strain (e.g., Nelson et al., 1992). The areas of mechanical interactions between extensional segments are structurally complex, including discrete zones of strike– and oblique–slip faults and/or wide regions of deformation characterised by overlapping fault terminations (see Peacock et al., 2000). Several works highlighted the coincidence of magmatic processes at transfer zones: examples include the East African Rift System (Rosendahl, 1987; Ebinger, 1989; Ebinger et al., 1989; Hayward and Ebinger, 1996), the Rio Grande Rift (Chapin and Chater, 1994), the Oslo Rift (Bartley, 1995) and the basin and range province (Faulds and Varga, 1998 and references therein). However, the processes that cause magmatic activity to concentrate at transfer zones, as well as the dynamic relations between the presence of magma and deformation in these structurally complex areas, are not well defined. Indeed, the relations between magmatism and deformation at transfer zones may be viewed as either a pre-existing magma body controlling the transfer zone location and structural pattern, or a pre-existing transfer zone controlling the magma migration (e.g., Ruppel, 1995; Faulds and Varga, 1998).

In this study, we simulated the development of a transfer zone progressively propagating across a pre-existing magma body that is assumed to have underplated the continental crust, as occurs beneath continental rift systems (e.g., Parsons et al., 1992; Olsen and Morgan, 1995). Doing so, we have focused our investigations on magma intrusions in a crustal-scale brittle–ductile system undergoing extension. Particularly, we present six-scaled centrifuge models designed to explore the dynamic relations between magma intrusions and strain distribution, focusing on the processes that cause magma emplacement in the lower crust to concentrate along transfer zones.

2. Experimental procedure, materials and scaling

2.1. Experimental setting

Experiments were performed at the Hans Ramberg Tectonic Laboratory (Uppsala University) by using the large-capacity centrifuge (Ramberg, 1981) in which $7\times7\times1.9$ cm models, built in a Plexiglas box, were accelerated to gravitational forces at about $200\times g$. During the experiments, we extended two halves of the models in opposite directions in order to reproduce two distinct rift segments with opposite border faults polarity (e.g., Serra and Nelson, 1988; Fig. 1). With this set-up, the central part of the model acted as a transfer zone linking the two rift segments and thus, accommodating the imposed differential movement (Fig. 1). Notably, this set-up created a central velocity discontinuity (VD) that, however, did not correspond to a discrete VD as that resulting in case of models built above moving rigid plates (e.g., Allemand et al., 1989). In this setting, the imposed extension direction is roughly parallel to the long side of the Plexiglas wall, although a local reorientation of the stress field may occur approaching the transfer zone (see the following: Experimental results and Discussion). Hereafter, the term extension direction indicates the imposed direction of the extension vector, representing the regional minimum principal stress (σ_3) that drives deformation in nature.

Extension was controlled by sequentially removing thin slices of confining Plasticine to allow the brittle–ductile system to expand into the open space (Fig. 1): we allowed the models to stretch laterally at increments of about 3.5 mm during 30-s intervals, which corre-

Fig. 1. Cartoon showing the sequential deformation of models TrZn4 (a–f), TrZn2 (g–m) and TrZn3 (n–s). Experimental set-up (a–b, g–h, n–o), initial strength profiles (c, i, p), sequential top-view line drawings of the main deformation steps (d–e, j–k, q–r) and models cross-section (f, m, s). In models TrZn2 and TrZn3, the initial position of the glycerol reservoir is indicated. Note that in the experimental procedure, two narrow bands of silicone (1-cm width) were placed at the extremities of the sand layer in order to confine it and to prevent the collapse of sand once the confining plasticine is removed. Numbers indicate the progressive development of faults. The black arrows indicate the imposed extension direction that is roughly parallel to longer side of the box; the rotation of the main structures approaching the transfer zone points to a local stress field reorientation. Grey dashed lines represent the passive grid markers. Dashed rectangular boxes indicate the inferred location of the transfer zones, which are formed by structures developed to accommodate the imposed differential movement between the two halves of the model. The β factor has been computed as the ratio between the final and initial length of the model brittle crust. UC: upper crust (sand); LC: lower crust (sand–silicone mixture); UM: upper mantle (high-density sand–silicone mixture); lvm: low-viscosity material (glycerol); GR: initial glycerol reservoir.

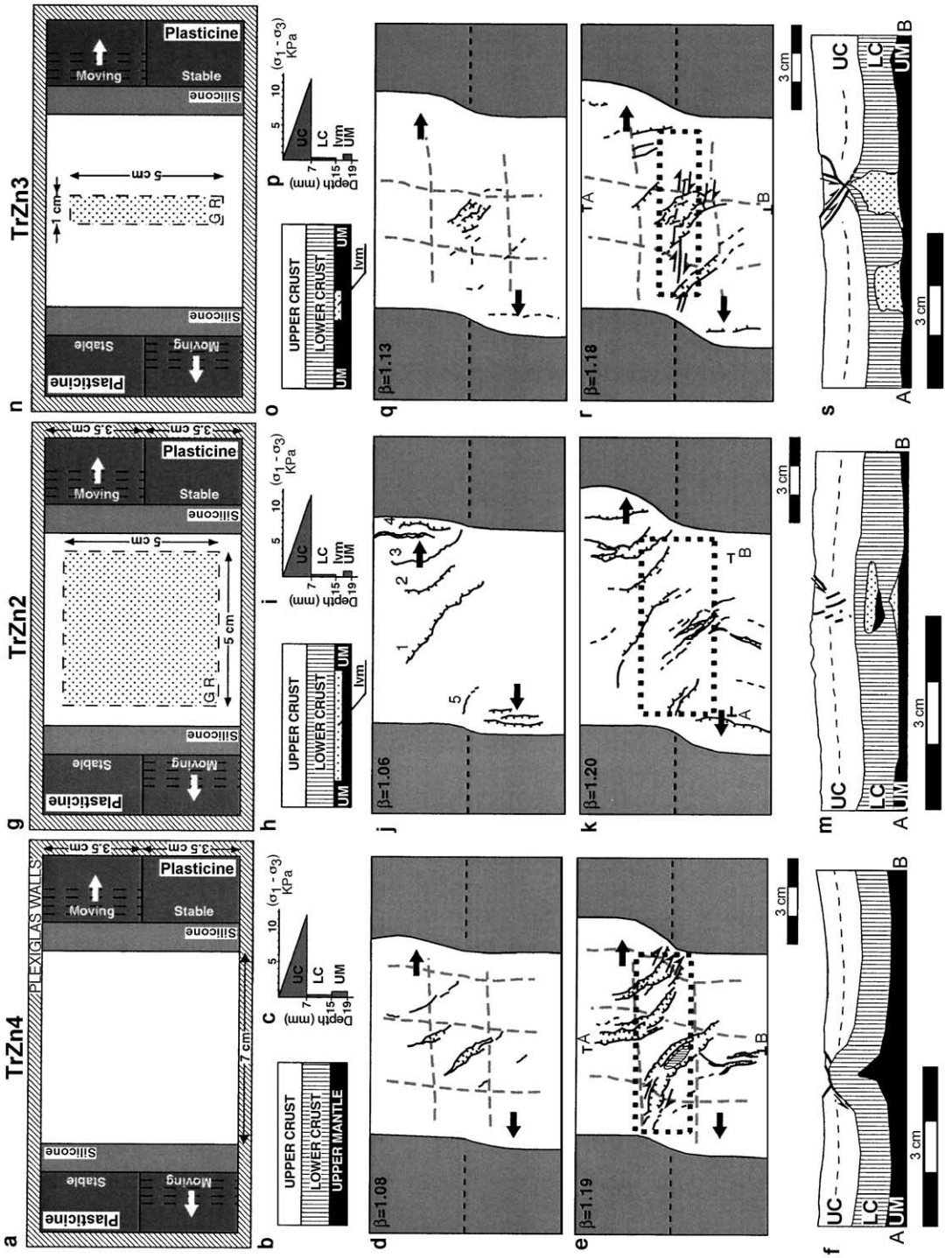
TrZn4
TrZn2
TrZn3
PLEXIGLAS WALLS
Plasticine
Moving
Stable
Silicone
3.5 cm
7 cm
5 cm
1 cm
UPPER CRUST
LOWER CRUST
UPPER MANTLE
UC
LC
UM
lvm
Depth (mm)
(σ1 - σ3) KPa
β=1.08
β=1.06
β=1.20
β=1.19
β=1.13
β=1.18
3 cm

Table 1
Parameters of models deformation

Model	Glycerol reservoir geometry	Glycerol reservoir dimensions (cm)	Glycerol reservoir position[a]	Extension rate[b] (mm s^{-1})	Final amount of extension (β)[b]
TrZn2 (Set 2)	wide squared reservoir (WSR)	$5 \times 5 \times 0.2$	0, 0	1.2×10^{-1}	1.20
TrZn3 (Set 1)	narrow rectangular reservoir (NRR)	$5 \times 1 \times 0.2$	0, 0	1.2×10^{-1}	1.18
TrZn4	no glycerol	no glycerol	no glycerol	1.2×10^{-1}	1.19
TrZn5 (Set 3)	small squared reservoir (SSR)	$1.5 \times 1.5 \times 0.2$	0, 1.5	1.2×10^{-1}	1.17
TrZn9 (Set 3)	small squared reservoir (SSR)	$1.5 \times 1.5 \times 0.2$	−1.5, 1	1.1×10^{-1}	1.20
TrZn12 (Set 3)	small squared reservoir (SSR)	$1.5 \times 1.5 \times 0.2$	0, 0	1.1×10^{-1}	1.20

[a] Values are in centimeters and indicate the x and y initial position of the centre of the reservoir with respect to the centre of the model (see Fig. 5a).
[b] Both the extension rate and the final amount of extension (β) represent an average value measured considering a single extending half of the model.

spond to model extension rates of $\approx 1.2 \times 10^{-1}$ mm s^{-1} (Table 1). The lateral edges and the bottom of the models were lubricated with liquid soap to provide free-slip boundaries, allowing deformation to be evenly distributed along the direction of extension. As a consequence, the brittle–ductile model was uniformly thinned in the central zone and the deformation of the brittle layer was driven by viscous traction at its base. In all models, the brittle layer was extended up to about 20% bulk extension (Table 1). After every successful experiment, the models were frozen before taking a number of cross-sections to study their 3-D internal geometry.

2.2. Materials

Following previous analogue works (Bonini et al., 2001; Corti et al., 2001), the characteristic strength profiles of the continental lithosphere were reproduced by using sand for the brittle layers and silicone–sand mixtures for the ductile behaviour of the lower crust and upper mantle. The rheological properties of these materials are summarised in Table 2. During the experiments, we simplified the initial rheological conditions in natural rifts assuming a magma body underplated at the base of the crust (e.g., Parsons et al., 1992; Olsen and Morgan, 1995). The occurrence of underplated magma also implies a high thermal state and a consequent "anomalous" ductile rheology for the upper mantle, although it still exhibits a higher resistance than the lower crust (see model strength profiles; Fig. 1c, i and p). Magma was reproduced in the experiments by using glycerol, which was mixed with a red pigment to enhance the colour contrast (see Table 2 for rheological properties).

Table 2
Characteristics of experimental materials

Prototype layer	Analogue material	Thickness (mm)	Density (kg m^{-3})	Coefficient of internal friction	Cohesion (Pa s)	Rheological characteristics	Viscosity (Pa s)
Upper crust	sand[a]	7	$\rho_{uc} = 1300$	$\mu = 0.6$	400	brittle behaviour	
Lower crust	sand + rhodorsil gomme 70009	8	$\rho_{lc} = 1500$			near-newtonian behaviour	$\approx 10^{5}$[b]
Upper mantle	sand + rhodorsil gomme 70009	4	$\rho_{um} = 1600$			near-newtonian behaviour	$\approx 5 \times 10^{5}$[b]
Magma	glycerol	2	$\rho_{m} = 1260$			newtonian behaviour	≈ 1[c]

[a] The sand was soaked with paraffin oil to enhance the cohesion and to avoid its collapse when introducing the models vertically in the centrifuge.
[b] Measured at the experimental strain rate of $\approx 10^{-3}$ s^{-1} and room temperature (≈ 23 °C).
[c] After Cruden et al. (1995).

2.3. Type of models

In order to model the influence on deformation of the underplated magma body, we designed different model set-up in which we changed the dimensions and the position of the initial (magma-simulating) glycerol reservoir (see Figs. 1, 5 and 6; Table 1). In particular, we performed three sets of experiments simulating the occurrence (in plan view) of a narrow rectangular reservoir (NRR, $1\times5\times0.2$ cm; Set 1, model TrZn3; Fig. 1n–s), a wide squared reservoir (WSR, $5\times5\times0.2$ cm; Set 2, model TrZn2; Fig. 1g–m) and a small squared reservoir (SSR, $1.5\times1.5\times0.2$ cm; Set 3, models TrZn5, 9 and 12; Figs. 5 and 6). The NRR and the WSR were placed in the middle of the model (Fig. 1), whereas different positions were investigated for the SSR (Figs. 5 and 6; Table 1). In all models, the glycerol reservoir was built below the upper mantle–lower crust interface (Figs. 1 and 5). For a comparison, one model (TrZn4; Fig. 1a–f) was performed without glycerol (Table 1).

2.4. Scaling

Geometrical similarity of our models was achieved by imposing a linear scaling factor of $h^* \approx 4.5\times10^{-7}$ (1 cm in the model corresponds to about 20 km in nature). This length ratio implies that the thickness of the initial glycerol reservoir scales down to $\approx$4-km thick magmatic underplating, a realistic value for extensional settings (e.g., Gans, 1987; Mechie et al., 1994).

Following Ramberg (1981), the condition of dynamic similarity between models and nature has been tested calculating dimensionless ratios of forces acting in the system. For the condition of dynamic similarity to be satisfied, these ratios are equal in the experiments and the natural prototype. For the viscous deformation, we calculated the ratio of gravitational to viscous stresses (Ramberg number; Weijermars and Schmeling, 1986)

$$R_m = \frac{\rho_d g h_d}{\eta \varepsilon} = \frac{\rho_d g h_d^2}{\eta V}$$

where ρ_d, h_d and η are the density, thickness and viscosity of the lower crust, g is the gravitational acceleration, ε is the experimental strain rate and V is the extension rate (see Table 3).

Analogously, we calculated the ratio of gravitational to cohesive stresses for the brittle deformation (see Ramberg, 1981; Mulugeta, 1988)

$$R_s = \frac{\rho_b g h_b}{\tau_c}$$

where ρ_b and h_b are the density and the thickness of the upper crust and τ_c is the cohesive strength (see Table 3). Since both models and nature share similar R_m and R_s numbers, we assume that experiments are dynamically scaled (Table 3). Particularly, assuming a reasonable lower crust viscosity in the order of 10^{21}–10^{22} Pa s, we can estimate that the models simulate an extension rate ranging between 2 and 20 mm year^{-1}, values that compare well with those estimated in natural extensional settings (e.g., in the Main Ethiopian Rift and Afar system; Hayward and Ebinger, 1996).

2.5. Simplifications of modelling

The present analogue modelling necessarily simplifies the investigated continental extension process, which is accompanied by important thermal and rheological variations. In particular, during our experiments, we could not reproduce the thermal effects induced by the emplacement of magma at the base or within the continental crust. This limitation prevents the possibility of taking into account thermal weakening of the country rocks, a mechanism which is invoked to influence rifting and strain localisation (e.g., Morley, 1999a,b). However, when considered in the light of the current models, these thermal effects are expected mostly to enhance strain localisation highligthed by the experimental results (see Discussion).

Beside the thermal effects, other simplifications concern the rheological characteristics of the underplated material. Particularly, glycerol is only five orders of magnitude less viscous than the silicone simulating the lower crust. Implying that when scaled to nature, glycerol is only able to simulate a crystal-rich magma ($\eta \approx 10^{16}$–10^{17} Pa s), not a crystal-free melt ($\eta \approx 10^{2}$–10^{6} Pa s; Clemens and Petford, 1999; Petford et al., 2000). This feature

Table 3
Scaling parameters of models and natural examples

ρ_d (lower crust density, kg m^{-3})	ρ_b (upper crust density, kg m^{-3})	g (gravitational acceleration, m s^{-2})	h_d (lower crust thickness, m)	h_b (upper crust thickness, m)	μ (coefficient of internal friction of the upper crust)	η (lower crust viscosity, Pa s)	V (extension rate, m s^{-1})	τ_c (cohesive strength, Pa)	$R_m = \frac{\rho_d g h_d^2}{\eta V}$	$R_s = \frac{\rho_b g h_b}{\tau_c}$
Models 1500	1300	1962	8×10^{-3}	7×10^{-3}	0.6	10^5	1.1×10^{-4}	400	17	44
Nature 2900	2700	9.81	1.8×10^4	1.6×10^4	0.6	$10^{21}-10^{22}$	6×10^{-10} -6×10^{-11}	10^7	15	42

Scaling parameters refer to the onset of deformation. Natural brittle parameters computed according to Byerlee's criterion.

affects the mechanism of magma transfer within the lower crust because the relatively high viscosity allows the glycerol to rise upwards, mostly in a diapiric way rather than to penetrate the lower crust as narrow sills or dykes (e.g., Ramberg, 1971). This means that our models, mainly accounting for only one (i.e., diapirism) of the three main mechanisms which explain magma transfer into the continental crust (e.g., dyking, pervasive transport through shear zones and diapirism; Petford et al., 2000), simplify the complex modalities of the natural process under investigation.

Since our investigations were exclusively focussed on the dynamic interactions between deformation into a transfer zone and the presence of a low-viscosity body introducing a rheological heterogeneity within the crust, we consider the current analogue simulations relevant despite the above mentioned simplifications.

3. Experimental results

3.1. Progressive deformation of models

In the model without magma-simulating glycerol (TrZn4), normal faults formed obliquely to the direction of extension and evolved in grabens that widened and lengthened, changing their trend during progressive extension (Fig. 1d and e). A complex transfer zone composed of oblique grabens developed to accommodate the differential movement between the two extending halves of the model. The final fault pattern is dominated by discrete grabens exhibiting a marked curvilinear trend (Fig. 1e). Along the central part of the model, in correspondence to the central VD, the grabens tend to parallel the direction of extension with the master faults showing a significant transcurrent component (see displacement of passive grid markers in Fig. 1e). Thinning of the upper crust resulted in the exhumation of the lower crust along an oblique dome emplaced within the major graben (Fig. 1e and f).

In Set 2 (model TrZn2), extension was accommodated by oblique normal faults that progressively affected the model surface, giving rise to a wide transfer zone characterised by diffuse deformation (Fig. 1j and k). This structural pattern resulted in a low amplitude doming within the ductile crust and a

limited upwelling of the layer simulating magma, which gave rise to a glycerol body (representing a magma chamber in nature) with a relatively high aspect ratio (Fig. 1m).

In Set 1 (model TrZn3), the first structure to develop was a graben trending obliquely to the direction of extension and located above the initial glycerol reservoir (Fig. 1q). With increasing stretching, a discrete strike–slip transfer fault formed in the centre of the model, then a new oblique graben developed at the left margin (Fig. 1r). A prominent uprising of glycerol occurred in the form of two domes above the pre-existing rectangular reservoir (Figs. 1c, 2, 3c and e). The major glycerol accumulation occurred along the transfer zone beneath the main graben, where the low-viscosity material raised above the brittle–ductile interface and ponded below the footwall of a major normal fault (Fig. 2c–d). 3-D analysis of the deformation of model TrZn3 (Fig. 3) shows that most of the deformation was localized within the transfer zone, which was characterized by high shear strain (Fig. 3a) and marked doming of the ductile crust (Figs. 3b–e and 4). The major glycerol accumulation (gb1 in Fig. 3c and e) was associated

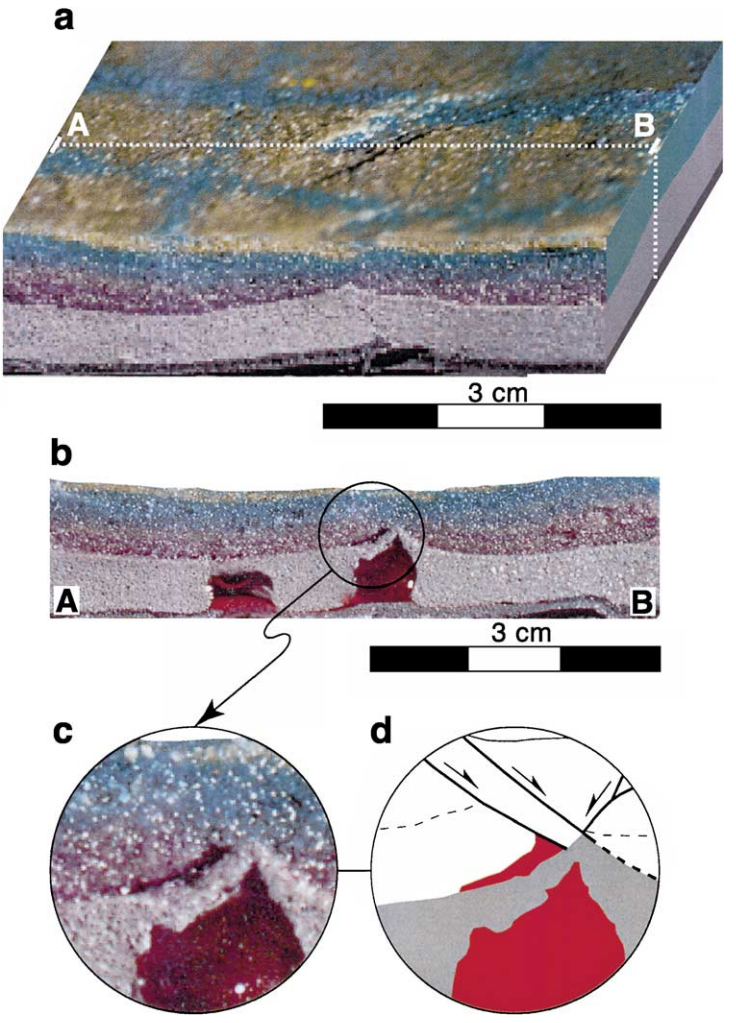

Fig. 2. (a) Final 3-D picture of model TrZn3. (b) Transversal section highlighting the two main glycerol bodies which emplaced above the initial reservoir. (c) Detail of the main glycerol body, with correspondent line-drawing (d), showing the uprising of the low-viscosity material at the brittle–ductile interface. Note that the glycerol at the base of the brittle crust is trapped below the footwall of a major normal fault.

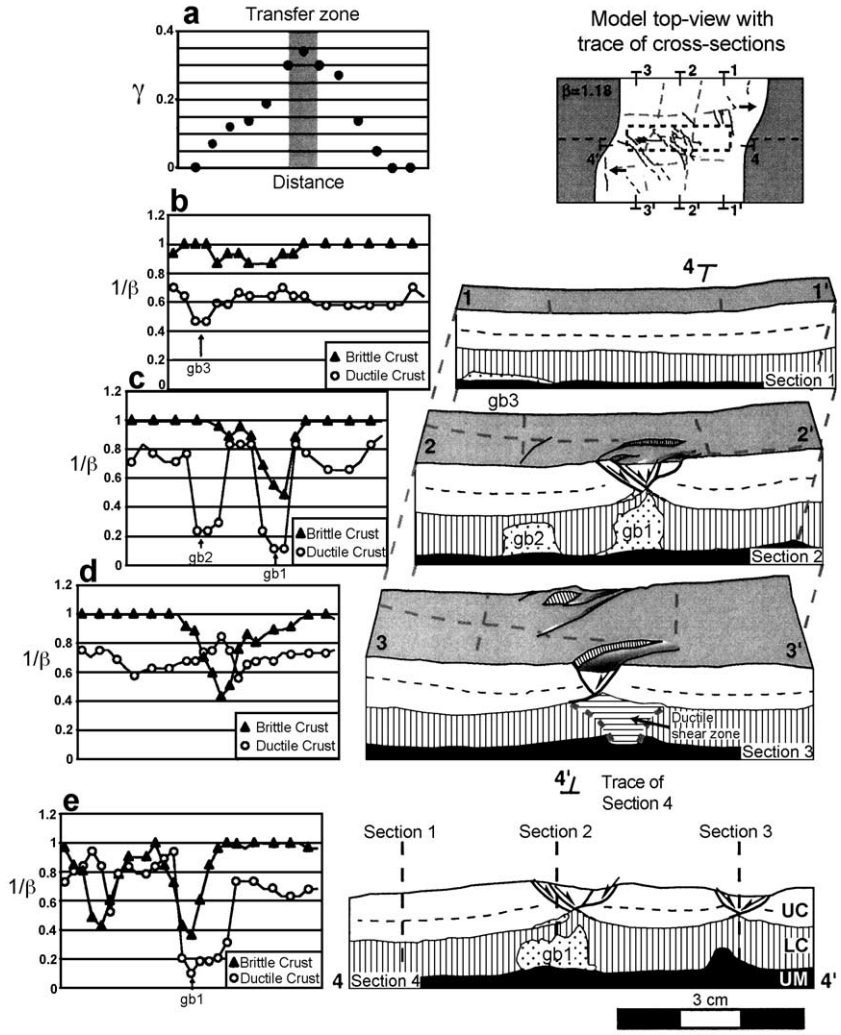

Fig. 3. 3-D structures of model TrZn3. (a) Variation in shear strain (expressed as $\gamma = \tan \phi$, where ϕ is angle of rotation of the extension–orthogonal passive grid markers) along section 2. (b)–(d) Transversal cross-sections. Traces of cross-sections are reported in a model top-view. Graphs on the left side indicate the variation of the $1/\beta$ value along the sections; $1/\beta$ is the ratio between the final and the initial thickness of the model crust ($1/\beta$ values less than 1 indicates thinning of the considered layer). gb: Glycerol body; other abbreviations as in Fig. 1. (e) Extension–parallel cross-section. In (c), the major glycerol body (gb1) is clearly associated with strong deformation of both brittle and ductile crust along the transfer zone, whereas the structural development of the other glycerol body (gb2) is rather enigmatic, being associated with no significant deformation in the upper crust. Possibly, gb2 developed in relation to the transfer zone-related differential movement segmenting the initial low-viscosity material reservoir and isolating discrete glycerol bodies within the lower crust.

with strong thinning of the upper crust (Fig. 3c) and doming of the ductile crust, whereas the other glycerol body (gb2) was associated a slight deformation in the upper crust with no significant rising of the brittle/ductile interface (see Figs. 3c and 4).

3.2. Magma-induced strain localisation

As described in the section above, during the first stages of deformation of model TrZn3, faults were concentrated in the central part of the model (in

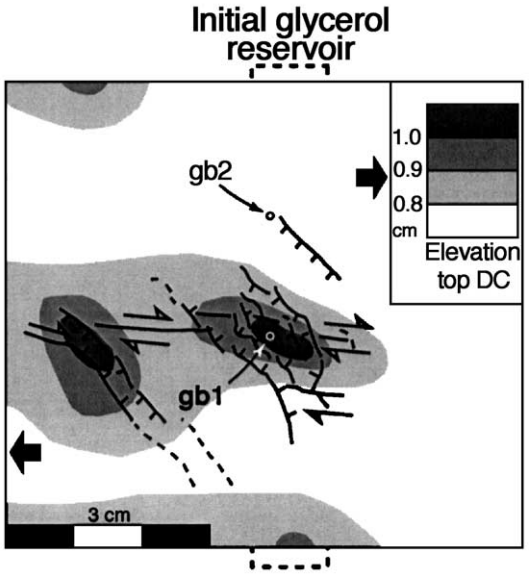

Fig. 4. Final fault pattern of model TrZn3 superimposed onto a map of the elevations of the top of the ductile crust. This map has been obtained removing the sand layer at the end of the experiment and measuring the elevations of the top of the ductile crust in several transversal and longitudinal cross-sections. Notice the oblique arrangement of domes in the ductile crust along the transfer zone. Small circles indicate the approximate position of the two major glycerol bodies (gb1 and gb2 as in Fig. 3).

correspondence to the VD) above the initial glycerol reservoir, suggesting the role played by the low-viscosity heterogeneity in localising strain in the overlying crust. This influence was further investigated by varying the initial position of the SSR in Set 3 models (TrZn5, 9 and 12; Figs. 5 and 6; Table 1).

Fig. 5 portrays the evolution of model TrZn9 which is taken as representative for this set of models. In a similar manner to model TrZn3 (Fig. 1q–r), deformation of model TrZn9 started with the development of an oblique narrow graben that typically formed in an eccentric position, coinciding at depth with the position of the initial small reservoir (Figs. 5b and 6b). With increasing extension, the deformation progressed with the lengthening of the oblique graben and the development, in correspondence of the central VD, of discrete strike–slip structures nucleating from the grabens extremities (Fig. 5c). As shown by the transversal cross-section reported in Fig. 5d, uprising of the glycerol occurred below the oblique graben, exhibiting a suspect dyking-like structure.

Models TrZn5 and TrZn12 also display a similar control of the glycerol reservoir on the position of the first surface structures (Fig. 6). Indeed, when the position of the SSR was varied, the grabens invariably formed in geometrical correspondence to the initial reservoir (Fig. 6).

These results clearly highlight that the presence of glycerol (i.e., magma) plays an important role on deformation by localising strain in the crust overlying

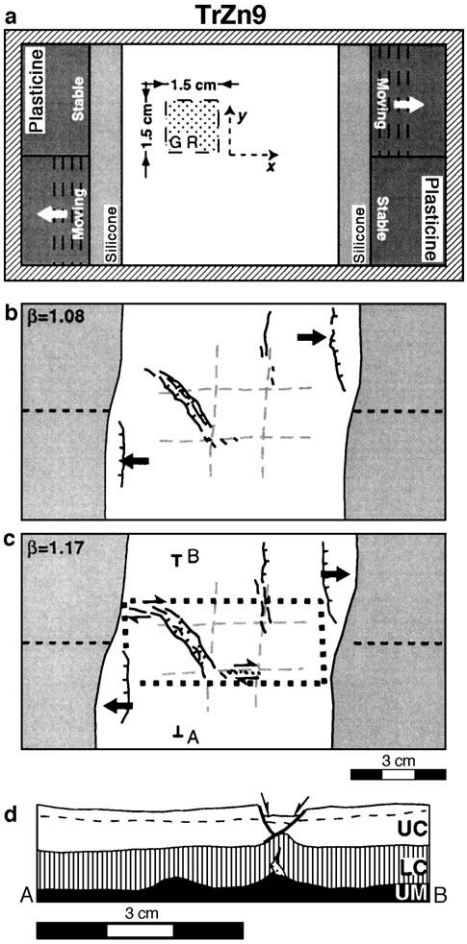

Fig. 5. Experimental set-up (a), sequential top-view line drawings of the main steps during deformation (b–c) and transversal cross-section (d) of model TrZn9. Note the suspect dyke-like glycerol intrusion below the central graben. The small mantle dome to the left of the glycerol accumulation might be associated with a deep-seated shear zone delimiting the main graben. The reference system used to indicate the position of the magma reservoir in Table 1 is indicated in (a). Symbols and abbreviations as in Fig. 1.

this low-viscosity body. This process is well evident at the initial stages of deformation, as shown in Fig. 6.

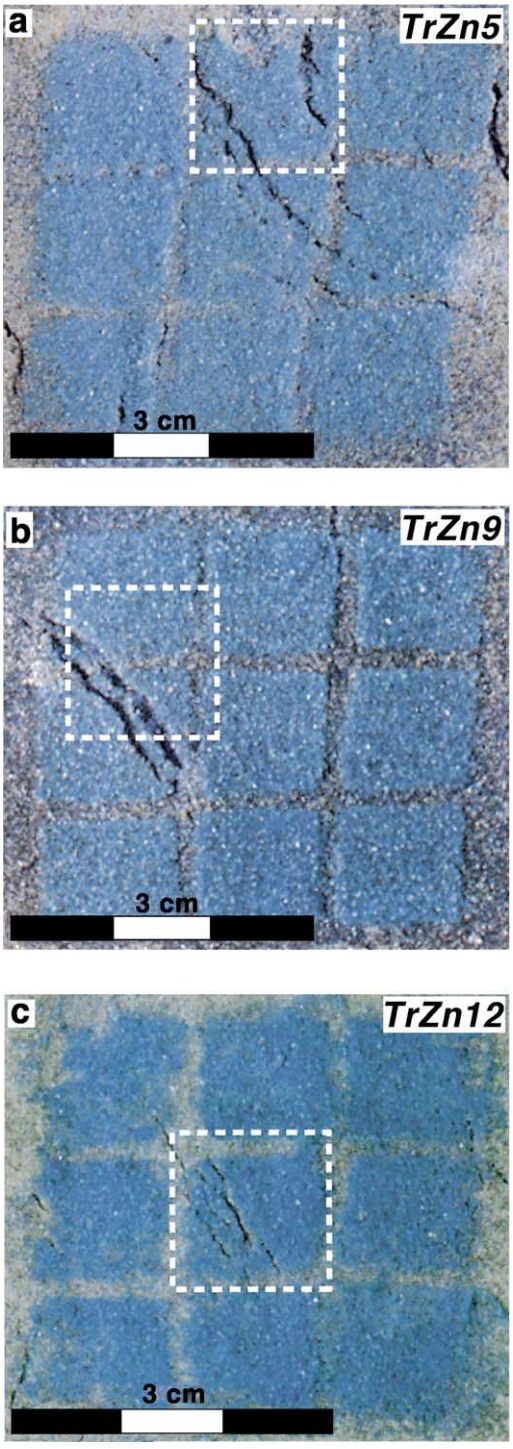

4. Discussion

The current analogue models reproduced a transfer zone propagating through an underplated glycerol reservoir. Thus, our models investigated magmatic intrusions in a crustal-scale brittle–ductile system, while previous analogue modelling studies focused on magma emplacement in the upper brittle crust in transpressional (Benn et al., 1998) and transtensional (Román-Berdiel et al., 2000) regimes. Introducing ductile heterogeneities into the lower crust represents therefore, an advance in physical modelling of transfer zones.

These experimental results show that in extensional settings, the strain distribution in the ductile and brittle crust is strongly controlled by the presence of magma at depth. The strain distribution, in turn, may control the size of magma upwelling (Figs. 1–5).

Similar to previous analogue modelling studies (e.g., Serra and Nelson, 1988; Basile and Brun, 1999), models without magma (e.g., TrZn4) show that deformation is accommodated by the development of normal faults that typically curve and increase their transcurrent component of movement approaching the central part of the model (i.e., the transfer zone). These faults border major crustal grabens which are markedly deflected approaching the central VD and the transfer zone. This pattern is consistent with a local reorientation of the extension direction in correspondence to the transfer zone, as documented in previous experimental works (e.g., Serra and Nelson, 1988; Acocella et al., 1999). Notably, ductile domes oblique to the extension direction formed within the graben depressions. On the other hand, models with glycerol at the base of the analogue crust provide valuable insights into the relations between the development of transfer zones and pre-existing magmas.

Fig. 6. Top-view pictures of model TrZn5 (a), TrZn9 (b) and TrZn12 at the early stages of extension (about 8% bulk extension; $\beta \approx 1.08$). The white dashed boxes indicate the initial position of the initial glycerol reservoir. Note that the initial grabens invariably formed above the initial reservoir.

Wide glycerol reservoir experiments (Set 2 models; TrZn2) are equivalent to an areally extensive underplating of magma. These models exhibit a diffuse deformation accompanied by a relatively limited glycerol upwelling that produced local magma chambers in the lower crust beneath the faulted upper crust (Fig. 1m). We suggest that this configuration would give rise to scattered volcanism coupled to the actual fault distribution.

Narrow glycerol reservoir (Set 1 models; TrZn3) and small reservoir experiments (Set 3 models; TrZn5, TrZn9 and TrZn12) simulate localized magmas beneath extending areas. In these cases, deformation notably started above the low-viscosity material, with the formation of an oblique graben. With increasing extension, deformation propagated along discrete strike–slip faults accommodating the transcurrent component along the transfer zone. On this basis, we interpret these grabens as pull-apart-like structures (see Figs. 1r and 5c). Shearing along the transfer zone and thinning of the brittle crust in the oblique grabens produced doming of the ductile crust (Fig. 1f) and favoured a marked glycerol upwelling (Fig. 1s), with the low-viscosity material collecting at the brittle–ductile interface below the footwall of major normal faults (Fig. 2c and d). This deformation pattern suggests that the emplacement of magmatic bodies may be strongly controlled by the rheological discontinuity between the upper and the lower crust, as also outlined by models on laccolith formation (Román-Berdiel et al., 1995). The process of emplacement is very similar to the "extensional footwall growth" model developed by Quirk et al. (1998), proposing that viscous fluids, such as magma or salt, preferentially migrate and collect in the low-stress zone in the normal fault footwall. Similar patterns of emplacement were obtained in previous experiments on magma intrusions in the brittle crust, also showing that strain and intrusions are strongly coupled during model deformation (Román-Berdiel et al., 2000).

The strong upwelling below the central pull-apart-like graben implies a lateral migration of glycerol toward the transfer zone, in a direction that is orthogonal to the imposed extension vector. Consequently, this process may account for the occurrence of significant magma accumulation into transfer zones. We suggest that model TrZn3 points to a striking relationship between strain localization, thinning of the brittle crust and important magma upwelling associated to ductile crust doming. In particular, the strong crustal strength reduction associated with a localized pre-existing magma is able to generate a perturbation in the strain field that propagates into the overlying crust (Arzi, 1978), facilitating strain localization and controlling the position and the structural pattern of transfer zones (Ruppel, 1995; Faulds and Varga, 1998). In the so-created areas of localized strain, important magma accumulation is expected, enhancing thermal softening of the country rocks and favouring further deformation (e.g., Morley, 1999a,b). This process may lead to a positive feedback interaction between tectonics and magmatism which has also been recognised in transpressional settings (e.g., Brown and Solar, 1998), as well as during post-orogenic collapse (McCaffrey et al., 1999).

4.1. Comparison with nature

In the current modelling we have investigated, in general terms, a process involving the mutual dynamic interactions between deformation and magma emplacement during the development of a transfer zone. Therefore, the results of modelling may be applied to a wide range of structural settings, such as transfer zones connecting different continental rift segments, or developing within single rift depressions. However, before comparing the results of modelling to nature, we draw attention to the fact that the structures in the models formed after the generation of underplated magma. Therefore, this model evolution would be better applied to active rifting processes, although model results may provide clues even in case of magmatic underplating related to an advanced passive rifting stage. Furthermore, in the comparison of models with nature, other limitations may concern the initial geometry of the magma layer, whose extent may vary during successive stages of rifting (e.g., Morley, 1994, 1999a), as well as the occurrence of large volumes of volcanic rocks that may prevent the observation of early structures. Additionally, no anisotropy has been introduced in the models, whereas in nature, reactivation of pre-existing fabrics in the brittle crust may play a major role during extension (e.g., Morley, 1999c).

Wide reservoir models (Set 2) can be compared with the transfer zone between the southern Main

Ethiopian Rift (MER) and the northern Kenya Rift (KR) in the East African Rift System (EARS), where large volumes of flood basalts erupted at the beginning of rifting suggest significant amounts of magma underplating (Braile et al., 1995; Prodehl et al., 1997). Similar to results of model TrZn2 (Fig. 1j–k), the diffused deformation within this ~300-km wide E–W transfer zone (Morley, 1999b; Morley et al., 1999; Ebinger et al., 2000; Fig. 7a) suggests that the width of this transfer zone may be related to widespread intrusions at the base of the ductile crust (e.g., Morley et al., 1999). Underplating beneath the Lake Turkana and the northern end of the Kenya Rift has indeed been imaged in seismic profiles in the form of a relatively high-velocity lower crust layer (e.g., Prodehl et al., 1997).

Narrow reservoir models (Set 1) may be applied to transfer zones in the Western Rift (WR) of the EARS, where the volcanic products are almost one order of magnitude less than those erupted in the KR (Braile et al., 1995) suggesting a limited underplating that is also hypothesised on the base of seismic data (Prodehl et al., 1997). In the WR, the distinct volcanic provinces coincide with major transfer zones, characterized by oblique to strike–slip faults (Rosendahl, 1987; Ebinger, 1989; Fig. 7b). Similar to our models, this concentration of magma at transfer zones may be driven by a lateral migration of magma, in a direction that is orthogonal to the regional extension direction.

Concerning the models deformed without glycerol at the base of the analogue crust, they may be applied to natural areas undergoing extension where underplated magma is absent or its influence on large-scale deformation is negligible. Notably, the fault pattern of model TrZn4 strikingly matches that observed in transfer zones on passive continental margins, such as the United Kingdom Continental Shelf (Fig. 7c, compare with Fig. 1e).

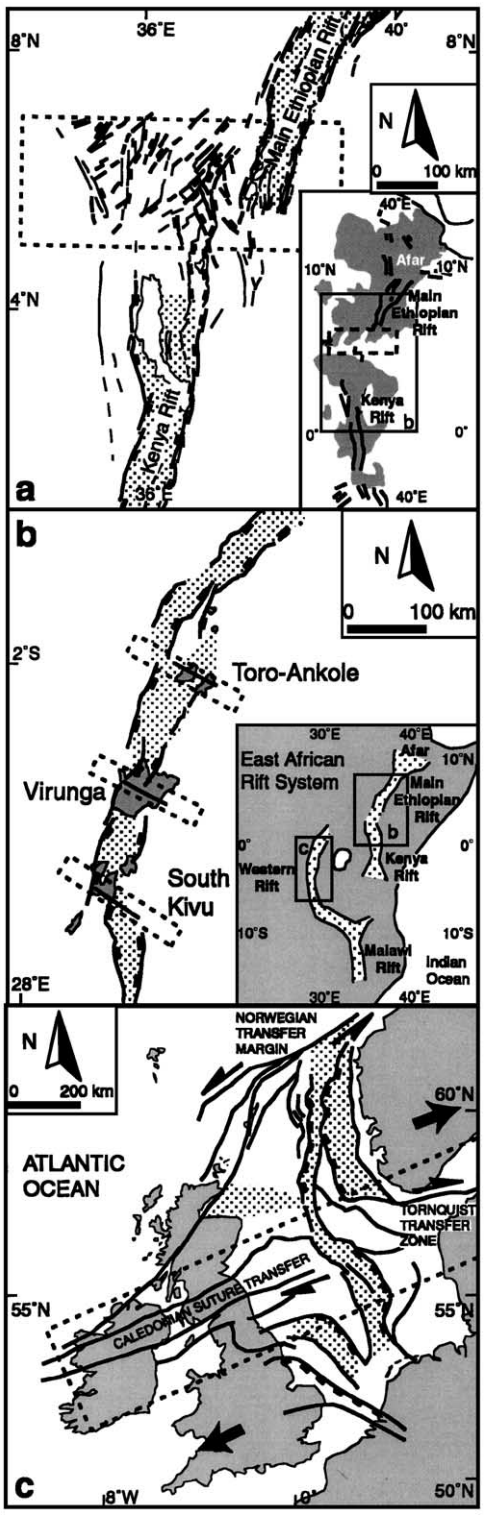

Fig. 7. Natural examples of transfer zones. (a) Distributed deformation between the Main Ethiopian Rift and the Kenya Rift (after Moore and Davidson, 1978). Inset shows the distribution of Eocene–Quaternary volcanic rocks. (b) Transfer zones in the Western Rift of the EARS (after Rosendahl, 1987; Ebinger, 1989). (c) Structural pattern in the United Kingdom Continental Shelf and adjacent areas (after Gibbs, 1989). Stippled and dark greyed areas represent rift depressions and volcanic rocks, respectively. Dashed rectangular boxes indicate the inferred location of the transfer zones. Notice the concentration of volcanism along the transfer zones in (b).

5. Conclusions

Centrifuge scaled models suggest the following main conclusions:

(1) Distribution of magma at depth can effectively control the strain distribution in the overlying continental crust and the evolution and the structural pattern of transfer zones. Narrow magma reservoirs result in a localized deformation accommodated by the development of discrete transfer faults, whereas areally extensive magma underplating results in a distributed deformation over a broad area.

(2) The presence of magma at depth in extensional settings can play a major role in controlling the structural evolution, representing therefore, an important parameter that must be taken into account in the study of such processes (see also Morley, 1999a,b).

(3) Magma-induced strain distribution may in turn control magma uprising: distributed deformation would result in scarce magma upwelling, whereas concentrated deformation is expected to localize magmatism into the transfer zone by favouring magma uprising and accumulation.

Acknowledgements

We thank the journal reviewers K.J.W. McCaffrey, T. Roman-Berdiel and O. Dauteuil and the Editor in Chief, J.P. Burg, for the stimulating and constructive criticism, which helped to improve this manuscript. We are also indebted with A.R. Cruden, C.K. Morley and G. Musumeci for fruitful suggestions on an earlier version of the manuscript. Research was sponsored by CNR and MURST (responsibles F. Innocenti and P. Manetti) grants. D. Sokuotis wishes to thank ISES (the Netherlands Centre for Integrated Earth Science) for financial support. G. Corti was partially supported by Progetto Giovani Ricercatori-CNR-Agenzia 2000.

References

Acocella, V., Faccenna, C., Funiciello, R., Rossetti, F., 1999. Sandbox modelling of basement-controlled transfer zones in extensional domains. Terra Nova 11, 149–156.

Allemand, P., Brun, J.P., Davy, P., Van Den Driessche, J., 1989. Symétrie et asymétrie des rifts et mécanismes d'amincissement de la lithospère. Bulletin de la Societe Geologique de France 8, 445–451.

Arzi, A.A., 1978. Critical phenomena in the rheology of partially melted rocks. Tectonophysics 44, 173–184.

Bartley, J.M., 1995. Magmatism and extension in the great basin and the Oslo rift: implications for rift mechanisms and segmentation. Geological Society of America Abstracts with programs 27, 120.

Basile, C., Brun, J.P., 1999. Transtensional faulting patterns ranging from pull-apart basins to transform continental margins: an experimental investigation. Journal of Structural Geology 21, 23–37.

Benn, K., Odonne, F., Saint-Blanquat, M., 1998. Pluton emplacement during transpression in brittle crust: new views from analogue experiments. Geology 26, 1079–1082.

Bonini, M., Sokoutis, D., Mulugeta, G., Boccaletti, M., Corti, G., Innocenti, F., Manetti, P., Mazzarini, F., 2001. Dynamics of magma emplacement in centrifuge models of continental extension with implications for flank volcanism. Tectonics 20, 1053–1065.

Braile, L.W., Keller, G.R., Wendlandt, R.F., Morgan, P., Khan, M.A., 1995. The East African rift system. In: Olsen, K.H. (Ed.), Continental Rifts: Evolution, Structure, Tectonics. Developments in Geotectonics, vol. 25, Elsevier, Amsterdam, 213–231.

Brown, M., Solar, G.S., 1998. Shear-zone systems and melts: feedback relations and self-organization in orogenic belts. Journal of Structural Geology 20, 211–227.

Chapin, C.E., Chater, S.M., 1994. Tectonic setting of the axial basins of the northern and central Rio Grande rift. In: Keller, G.R., Chater, S.M. (Eds.), Basins of the Rio Grande Rift: Structure, Stratigraphy, and Tectonic Setting. Geological Society of America Special Paper, vol. 291, Geol. Soc. Am., Boulder, CO, pp. 5–25.

Clemens, J.D., Petford, N., 1999. Granitic melt viscosity and silicic magma dynamics in contrasting tectonic settings. Journal of the Geological Society (London) 156, 1057–1060.

Corti, G., Bonini, M., Innocenti, F., Manetti, P., Mulugeta, G., 2001. Centrifuge models simulating magma emplacement during oblique rifting. Journal of Geodynamics 31, 557–576.

Cruden, A.R., Koyi, H., Schmeling, H., 1995. Diapiric basal entrainment of mafic into felsic magma. Earth and Planetary Science Letters 131, 321–340.

Ebinger, C.J., 1989. Geometric and kinematic development of border faults and accommodation zones, Kivu-Rusizi rift, Africa. Tectonics 8, 117–133.

Ebinger, C.J., Deino, A.L., Drake, R.E., Tesha, A.L., 1989. Chronology of volcanism and rift basin propagation: Rungwe Volcanic Province, East Africa. Journal of Geophysical Research 94, 15785–15803.

Ebinger, C.J., Yemane, T., Harding, D.J., Tesfaye, S., Kelley, S., Rex, D.C., 2000. Rift deflection, migration, and propagation: linkage of the Ethiopian and eastern rifts, Africa. Geological Society of America Bulletin 112, 163–176.

Faulds, J.E., Varga, R.J., 1998. The role of accommodation zones and transfer zones in the regional segmentation of extended terranes. In: Faulds, J.E., Stewart, J.H. (Eds.), Accommodation

Zones and Transfer Zones: the Regional Segmentation of the Basin and Range Provinces. Geological Society of America Special Paper, vol. 323, Geol. Soc. Am., Boulder, CO, pp.1–45.
Gans, P.B., 1987. An open-system, two-layer crustal stretching model for the eastern Great Basin. Tectonics 6, 1–12.
Gibbs, A.D., 1989. A model for linked basin development around the British isles. In: Tankard, A.J., Balkwill, H.R. (Eds.), Extensional Tectonics and Stratigraphy of the North Atlantic margins American Association of Petroleum Geologists Memoir, vol. 46, The Am. Assoc. of Petr. Geol., Tulsa, OK, pp. 81–93.
Hayward, N.J., Ebinger, C.J., 1996. Variations in the along-axis segmentation of the Afar Rift system. Tectonics 15, 244–257.
McCaffrey, K.J.W., Miller, C.F., Karlstrom, K.E., Simpson, C., 1999. Synmagmatic deformation patterns in the Old Woman Mountains, SE California. Journal of Structural Geology 21, 335–349.
Mechie, J., Keller, G.R., Prodehl, C., Gaciri, S.J., Braile, L.W., Mooney, W.D., Gajewski, D., Sandmeier, K.J., 1994. Crustal structure beneath the Kenya Rift from axial profile data. Tectonophysics 236, 179–200.
Moore, J.M., Davidson, A., 1978. Rift structure in southern Ethiopia. Tectonophysics 46, 159–173.
Morley, C.K., 1994. Interaction of deep and shallow processes in the evolution of the Kenya Rift. Tectonophysics 236, 81–91.
Morley, C.K., 1999a. Tectonic evolution of the East African Rift System and the modifying influence of magmatism: a review. Acta Vulcanologica 11, 1–19.
Morley, C.K., 1999b. Basin evolution trend in East Africa. In: Morley, C.K. (Ed.), Geoscience of Rift Systems—Evolution of East Africa. American Association of Petroleum Geologists Studies in Geology, vol. 44, The Am. Assoc. of Petr. Geol., Tulsa, OK, pp. 131–150.
Morley, C.K., 1999c. How successful are analogue models in addressing the influence of pre-existing fabrics on rift structures? Journal of Structural Geology 21, 1267–1274.
Morley, C.K., Karanja, F.M., Wescott, W.A., Stone, D.M., Harper, R.M., Wigger, S.T., Day, R.A., 1999. Geology and geophysics of the western Turkana Basins. In: Morley, C.K. (Ed.), Geoscience of Rift Systems—Evolution of East Africa. American Association of Petroleum Geologists Studies in Geology, vol. 44, The Am. Assoc. of Petr. Geol., Tulsa, OK, pp. 19–54.
Mulugeta, G., 1988. Squeeze box in a centrifuge. Tectonophysics 148, 323–335.
Nelson, R.A., Patton, T.L., Morley, C.K., 1992. Rift-segment interaction and its relation to hydrocarbon exploration in rift systems. American Association of Petroleum Geologists Bulletin 74, 1153–1169.
Olsen, K.H., Morgan, P., 1995. Introduction: progress in understanding continental rifts. In: Olsen, K.H. (Ed.), Continental Rifts: Evolution, Structure, Tectonics. Developments in Geotectonics, vol. 25, Elsevier, Amsterdam, pp. 3–25.
Parsons, T., Sleep, N.H., Thompson, G.A., 1992. Host rock rheology controls on the emplacement of tabular intrusions: implications for underplating of extending crust. Tectonics 11, 1348–1356.
Peacock, D.C.P., Knipe, R.J., Sanderson, D.J., 2000. Glossary of normal faults. Journal of Structural Geology 22, 291–305.
Petford, N., Cruden, A.R., McCaffrey, K.J.W., Vigneresse, J.-L., 2000. Granite magma formation, transport and emplacement in the Earth's crust. Nature 408, 669–673.
Prodehl, C., Fuchs, K., Mechie, J., 1997. Seismic-refraction studies of the Afro–Arabian rift system—a brief review. Tectonophysics 278, 1–13.
Quirk, D.G., D'Lemos, R.S., Mulligan, S., Rabti, M.R., 1998. Insights into the collection and emplacement of granitic magma based on 3D seismic images of normal fault-related salt structures. Terra Nova 10, 268–273.
Ramberg, H., 1971. Dynamic models simulating rift valleys and continental drift. Lithos 4, 259–276.
Ramberg, H., 1981. Gravity, Deformation and the Earth's Crust Academic Press, London.
Román-Berdiel, T., Brun, J.P., Gapais, D., 1995. Analogue models of laccolith formation. Journal of Structural Geology 17, 1337–1346.
Román-Berdiel, T., Aranguren, A., Cuevas, J., Tubía, J.M., Gapais, D., Brun, J.P., 2000. Experiments on granite intrusions in transtension. In: Vigneresse, J.L., Mart, Y., Vendeville, B. (Eds.), Salt, Shale and Igneous Diapirs in and Around Europe. Geological Society, London, Special Publications, vol. 174, The Geol. Soc., London, pp. 21–42.
Rosendahl, B.L., 1987. Architecture of continental rifts with special reference to east Africa. Annual Review of Earth and Planetary Sciences 15, 445–503.
Ruppel, C., 1995. Extensional processes in continental lithosphere. Journal of Geophysical Research 100, 24187–24215.
Serra, S., Nelson, R.A., 1988. Clay modelling of rift asymmetry and associated structures. Tectonophysics 153, 307–312.
Weijermars, R., Schmeling, H., 1986. Scaling of Newtonian and non-Newtonian fluid dynamics without inertia for quantitative modelling of rock flow due to gravity (including the concept of rheological similarity). Physics of the Earth and Planetary Interiors 43, 316–330.